Journal of Alloys and Compounds 509 (2011) 3403–3408

Contents lists available at ScienceDirect

Journal of Alloys and Compounds

journal homepage: www.elsevier.com/locate/jallcom

The synthesis of novel ZnO microcrystals through a simple solvothermal method and their optical properties

Zai-Xing Yang [a], Xin Du [a], Wei Zhong [a,*], Yan-Xue Yin [c], Mei-Hua Xu [a], Chaktong Au [b], You-Wei Du [a]

[a] Nanjing National Laboratory of Microstructures and Department of Physics, Nanjing University, Nanjing 210093, People's Republic of China
[b] Chemistry Department, Hong Kong Baptist University, Hong Kong, People's Republic of China
[c] Laser Institute, Qufu Normal University, Qufu 273165, People's Republic of China

ARTICLE INFO

Article history:
Received 19 August 2010
Received in revised form
13 December 2010
Accepted 15 December 2010
Available online 22 December 2010

Keywords:
Semiconductors
Chemical synthesis
Crystal growth
Luminescence

ABSTRACT

ZnO microcrystals with novel structures have been synthesized by a solvothermal method that is facile, low-cost and environment-friendly. $Zn(NO_3)_2{\cdot}6H_2O$ is the only precursor and absolute ethanol is the solvent. By controlling the reaction time, temperature and molarity of zinc nitrate, ZnO entities with the shape of flower, nut, hexagon-pillar, popcorn, brush and sphere can be synthesized in high selectivity. The ZnO micronuts (length ~8 μm and width ~5 μm) are uniform in morphology, displaying an open gap on the surface that divides the body into two. The investigation on the optical properties of the ZnO microcrystals reveals that all the ZnO samples exhibit an excitonic absorption edge around 376 nm, and compared to bulk ZnO, there is a modest red shift of ~6 nm that can be ascribed to size effect as well as the unique morphologies of the ZnO microcrystals.

1. Introduction

With the ever decreasing dimensions of devices used in catalysis, optical storage, light emitting display, energy conversion and storage, chemical and biological sensing and diagnosis, the growth of micro- and nano-structure materials in a controlled manner is getting more and more important [1]. In the academic sector, the systems are studied because the properties of nanomaterials can be significantly different from those of the bulk counterparts (a result of quantum-sized effects). As for the synthesis of nanomaterials, it is meaningful to adopt methods that are simple, efficient, and environment-friendly. From a commercial view point, low cost, high throughput, and ease of production (e.g., template-free) are favored factors. In our previous work, we prepared single-crystalline CdO and $Cd(OH)_2$ nanowires by a simple hydrothermal method using aqueous $Cd(NO_3)_2$ as the only precursor [2].

In the past decade, zinc oxide (ZnO) has been studied widely. The material exhibits wide band gap (3.37 eV), large exciton binding energy (60 meV), large electron mass (0.3 m_e; m_e denotes bare electron mass) and excellent chemical and thermal stability. With such properties, ZnO is used in areas such as optical absorption and emission [3], piezoelectricity [4], photocatalysis [5] and gas sensing [6]. Researches on the generation of nano- and micro-structure ZnO of various shapes have been conducted [7]. The popular routes for the fabrication of nano- and micro-structure ZnO are thermal evaporation [8], chemical vapor deposition (CVD) [9], metal–organic chemical vapor deposition (MOCVD) [10], pulsed laser deposition (PLD) [11] and template-based growth [12]. Looking into these approaches, one can realize that stringent requirements, e.g. vacuum techniques, high temperatures, complicated controlling processes and the use of catalysts and noxious compounds are often involved. In other words, the methods are not suitable for large-scale production in low cost.

Recently, solution-based solvothermal and hydrothermal methods were adopted for the synthesis of ZnO nano- and micro-materials. Overall, the approaches appear to be facile and promising. For example, Zeng et al. [13] generated nutlike ZnO microcrystals in large quantity through a low-temperature hydrothermal route that involved pH adjustment of the aqueous solution of zinc acetate dihydrate and triethanolamine (TEA). Through a surfactant-directed process using zinc nitrate, sodium dodecyl benzene sulfonate (SDBS) and sodium hydroxide as ingredients, Zhang et al. [14] produced hierarchical nanostructure of ZnO. Nonetheless, most of the reported solvothermal and hydrothermal methods for preparing ZnO involved the use of various reagents in specific amounts and the procedures required close monitoring.

Herein, we report a simple solvothermal method for the fabrication of ZnO microcrystals. In this approach, $Zn(NO_3)_2{\cdot}6H_2O$ is the precursor and absolute ethanol is the solvent, and there is no need to use a surfactant. By varying the reaction time, temperature and concentration of zinc nitrate, the growth of ZnO microcrystals can

* Corresponding author. Tel.: +86 25 83621200; fax: +86 25 83595535.
E-mail address: wzhong@mail.nju.edu.cn (W. Zhong).

0925-8388/$ – see front matter © 2010 Elsevier B.V. All rights reserved.
doi:10.1016/j.jallcom.2010.12.089

Table 1
Optimal conditions for the generation of ZnO microcrystals.

Morphology	$Zn(NO_3)_2{\cdot}6H_2O$ molarity (mol/L)	Heating time (h)
Sphere	0.03	24
Brush	0.05	24
Popcorn	0.08	24
Flower	0.1	1
Nut	0.1	10
Hexagon-pillar	0.5	24

be selectively controlled. To the best of our knowledge, the fabrication of ZnO microcrystals in such a manner has never been reported before.

2. Experimental

All the reagents were of analytical grade (purchased from NanJing Chemical Industrial Co.) and used without further purification. In a typical procedure [15], various amount of $Zn(NO_3)_2{\cdot}6H_2O$ were dissolved in absolute ethanol to form 40.0 mL solutions of different zinc concentrations. The solvothermal synthesis was conducted in an electric oven at 150 °C for a designated period of time. The optimal conditions for the generation of ZnO microcrystals are depicted in Table 1. After cooling naturally to room temperature (RT), the as-obtained solid was separated by centrifugation and washed thoroughly (five times) with absolute ethanol and deionized water.

The as-obtained materials were examined on an X-ray powder diffractometer (XRD) at RT for phase identification using Cu Kα radiation (Model D/Max-RA, Rigaku). The morphology of samples was examined over a high-resolution transmission electron microscope (HR-TEM, JEOL-2010, operated at an accelerating voltage of 200 kV) and a field emission scanning electron microscopy (FE-SEM, FEI Sirion 200, operated at an accelerating voltage of 5 kV). The optical properties of the materials were investigated for ultraviolet–visible (UV–vis) absorption (Cary, USA) and photoluminescence (PL, excitation source: He–Cd laser, 325 nm) at RT.

3. Results and discussion

Fig. 1 shows the XRD patterns of the materials fabricated under different conditions. Shown in Fig. 1a are the patterns of samples collected after different synthesis times with the amount of $Zn(NO_3)_2{\cdot}6H_2O$ fixed at 0.1 M (40 mL) and temperature at 150 °C. The sample of 0.5 h shows poor crystallinity. When the time reaches 1 h, $Zn(OH)_2$, ZnO and a kind of zinc compound in the form of $Zn_5(OH)_8(NO_3)_2(H_2O)_2$ (JCPDS no. 720627) can be detected. For the samples collected after 3, 24 and 48 h, the XRD patterns show the sole presence of wurtzite ZnO. As shown in Fig. 1b, with the rise of $Zn(NO_3)_2{\cdot}6H_2O$ molarity from 0.01 to 0.5 M and temperature from 150 to 200 °C, ZnO of hexagonal phase remains as the only product after 24 h. Based on the results, we suggest that the reaction steps involved are:

$$5Zn(NO_3)_2 + 10H_2O \rightarrow Zn_5(OH)_8(NO_3)_2(H_2O)_2 + 8HNO_3 \quad (1)$$

$$Zn_5(OH)_8(NO_3)_2(H_2O)_2 \rightarrow 5Zn(OH)_2 + 2HNO_3 \quad (2)$$

$$Zn(OH)_2 \rightarrow ZnO + H_2O \quad (3)$$

According to the FE-SEM images of Fig. 2a and d, flowerlike and nutlike microcrystals are synthesized at 150 °C and 0.1 M $Zn(NO_3)_2{\cdot}6H_2O$ in a period of 1 and 10 h, respectively. The microflowers are made up of flakes that are several micrometers in diameter and about 25 nm in thickness (Fig. 2a), and there is occasional sighting of nutlike particles on the flakes. The TEM image of an individual flake is shown in Fig. 2b. It is worth reporting that the microflowers were unstable under electron bombardment during HR-TEM observation, and readily decomposed into nanoparticles of 3–4 nm in size as depicted in Fig. 2c. In view of the instability of the microflowers, they can act as a kind of substrate for crystal growth of some kind. After 10 h of synthesis, nutlike ZnO particles are detected. The micronut is about 8 μm in length and 5 μm in width, and there is an open gap that divides the nut surface into two (Fig. 2d and e). As showed in the TEM image (Fig. 2e), the two halves of the nut are joint in the middle. According to the HR-TEM image (Fig. 2f), the lattice spacing is ~0.26 nm which is very close to the d_{002} lattice fringe of wurtzite ZnO. The selected area electron diffraction (SAED) pattern (inset of Fig. 2f) confirms the single crystallinity of ZnO micronut and suggests a growth direction along the c axis (i.e. the ⟨0 0 0 1⟩ direction).

In order to understand the growth mechanism of nutlike ZnO, we monitored the shape of intermediates with respect to time (15 min to 24 h) during synthesis (temperature = 150 °C, molarity of $Zn(NO_3)_2{\cdot}6H_2O$ = 0.1 M) (FE-SEM, Fig. 3a–i). Before the beginning of the solvothermal process, the solution of $Zn(NO_3)_2{\cdot}6H_2O$ in absolute ethanol was transparent, indicating the complete dissolution of the former in the latter. After a solvothermal period of 15 min, agglomerates with irregular shape are formed (Fig. 3a). After 30 min, flowerlike agglomerates (getting bigger in size) composed of flakes are detected (Fig. 3b and c), and there are particles of around 110 nm in size on the flake. After 1 h (Fig. 3d), flowerlike and nutlike microcrystals coexist, with the former being irregular in shape. After 3 h (Fig. 3e), the flowerlike entities disappear completely and there is the appearance of prototype micronuts. At this stage, the gap that divides the nut surface into two can already be seen. In Fig. 3f, one can see that small nanorods are sprouting outwards. It is clear that the micronut is not a simple aggregation of small nanoparticles but an entity that is composed of nanowires grown on a common interface. After 10 h, the ZnO micronuts are ca. 8 μm in length and ca. 5 μm in width (Fig. 3g). Shown in Fig. 3h is the top view of a ZnO micronut; one can see that the segment (rather compact but slightly porous in texture) fuses to a central core. At 24 h (Fig. 3i), acornlike ZnO micronuts are formed; the two

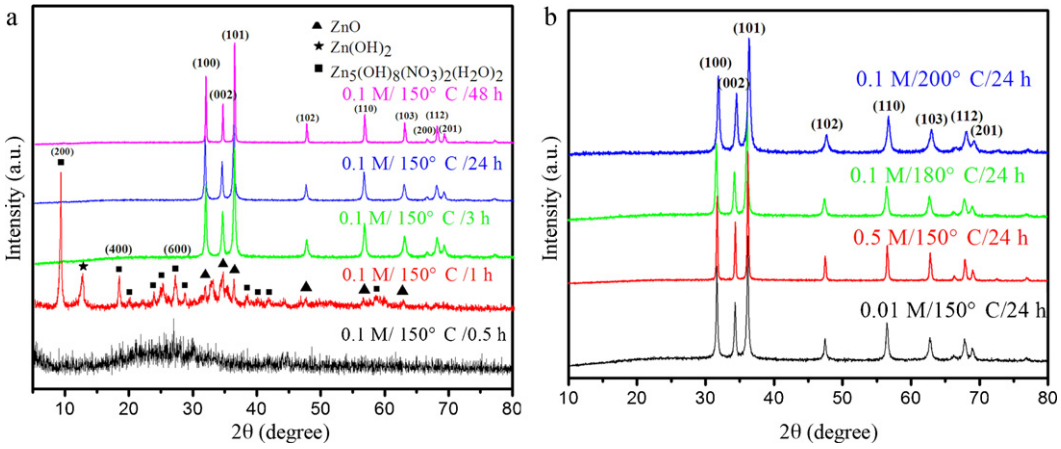

Fig. 1. XRD patterns of the materials fabricated under different conditions (asterisk: $Zn(OH)_2$; triangle: ZnO; square: $Zn_5(OH)_8(NO_3)_2(H_2O)_2$).

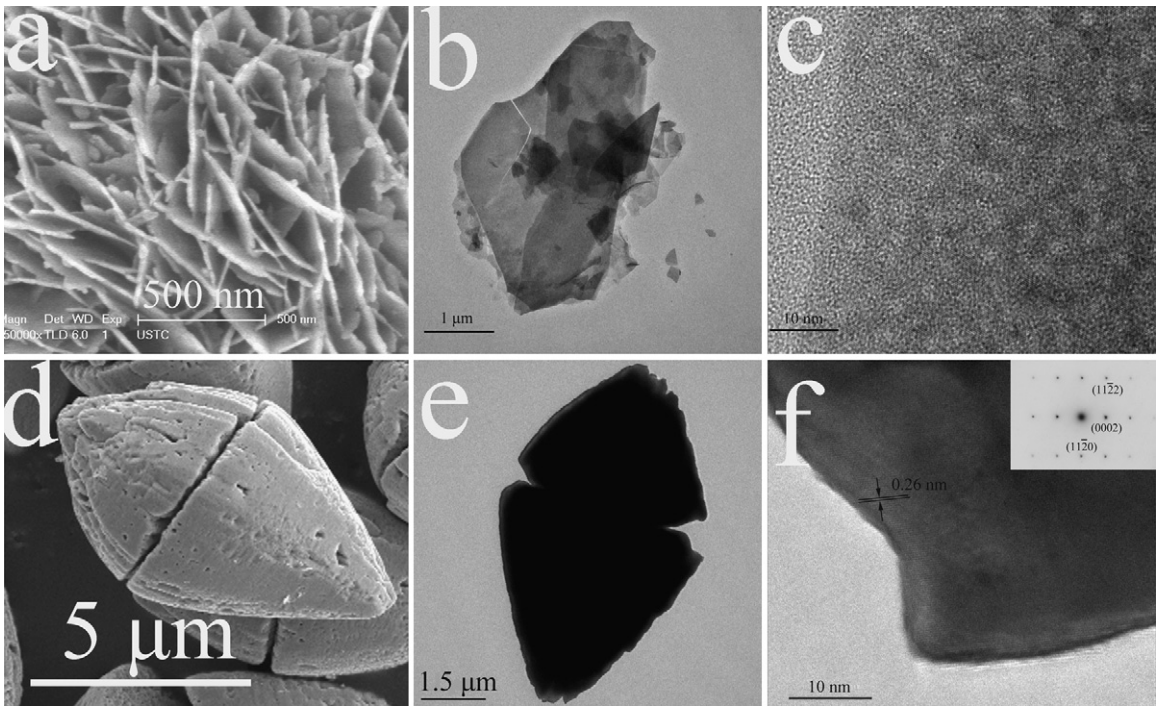

Fig. 2. (a) FE-SEM image of microflower synthesized at 150 °C and 0.1 M $Zn(NO_3)_2{\cdot}6H_2O$ in 1 h; (b and c) TEM and HR-TEM images of a flake of microflowers; (d and e) FE-SEM and TEM images of a ZnO micronut synthesized at 150 °C and 0.1 M $Zn(NO_3)_2{\cdot}6H_2O$ in 10 h; (f) HR-TEM image and SAED pattern (inset) of a ZnO micronut.

halves of the nut fused completely and the surface of the nut is smooth.

Although the exact mechanism for the growth of ZnO micronuts is unclear, one can make certain deduction based on known information in the literature [16–18]. It is known that the final morphology of a crystal is mainly determined by its intrinsic crystallinity. Nonetheless, factors such as solvent, pH value, temperature, time for crystallization and capping reagent have effects on its final appearance. Shown in Fig. 4 is the growth schema of ZnO micronuts. During the initial stage of the solvothermal synthesis,

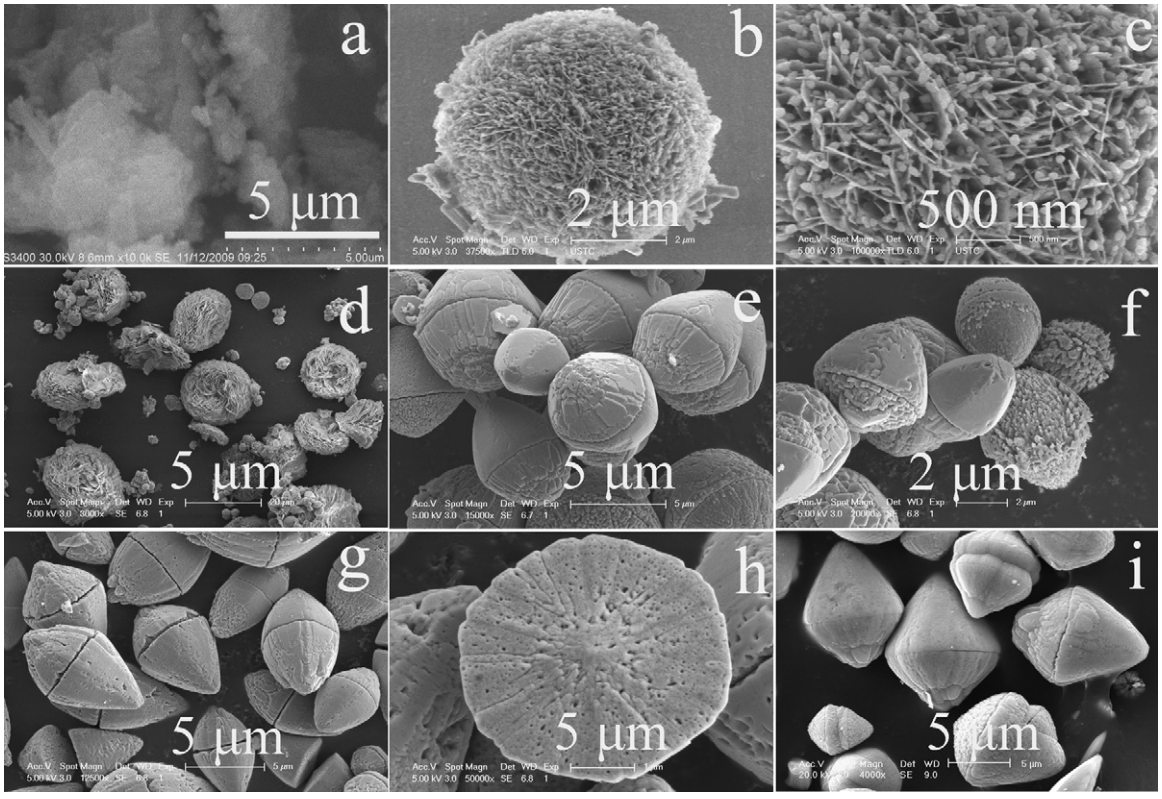

Fig. 3. FE-SEM images of ZnO micronuts collected after synthesis of (a) 15 min, (b and c) 0.5 h, (d) 1 h, (e and f) 3 h, (g and h) 10 h and (i) 24 h. (temperature = 150 °C, molarity of $Zn(NO_3)_2{\cdot}6H_2O$ = 0.1 M).

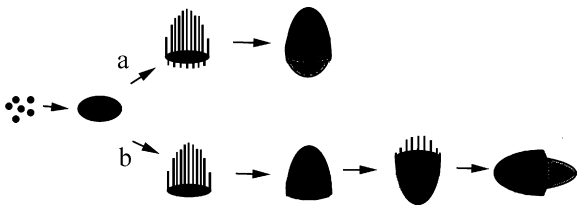

Fig. 4. Growth schema of ZnO micronuts.

layered $Zn_5(OH)_8(NO_3)_2(H_2O)_2$ and $Zn(OH)_2$ with sheetlike morphology (Fig. 3b and c) are generated. Then there is the growth of ZnO nanorods on the $Zn_5(OH)_8(NO_3)_2(H_2O)_2$ and $Zn(OH)_2$ sheets (as shown in Fig. 3f). With time, $Zn_5(OH)_8(NO_3)_2(H_2O)_2$ and $Zn(OH)_2$ dissolve away (based on the results of XRD (Fig. 1) and FE-SEM (Fig. 3d and e)), leaving behind the ZnO nanorods. A similar picture was depicted by Gautam et al. [16] for the solvothermal synthesis of pure and N-doped ZnO nanobullets. Furthermore, according to Govender et al. [17], the growth rate (V) of crystal in solution along a plane usually follows the order of: $V(0\,0\,0\,1) > V(\bar{1}\,0\,1\,\bar{1}) > V(\bar{1}\,0\,1\,0) > V(\bar{1}\,0\,1\,1) > V(0\,0\,0\,\bar{1})$. With fastest crystal growth along the $\langle 0\,0\,0\,1\rangle$ (i.e. the c axis) direction and slowest growth along the $\langle 0\,0\,0\,\bar{1}\rangle$ direction, there is the formation of ZnO rods. As depicted in Fig. 4a and b, there can be two kinds of ZnO crystal growth: (1) ZnO nanorods grow on both sides of a flake at different speeds (Path a), and (2) ZnO nanorods grow on one side of a flake at highest speed along the $\langle 0\,0\,0\,1\rangle$ direction (Path b). In the latter case, a half nut is first formed and then the base of the half nut acts as a seed layer for another phase of nanorod growth as illustrated before by Greene et al. [18] (giving a step morphology on the surface). In both cases, the asymmetric micronuts (rather than ellipsoidal) are formed. According to the SEM (Fig. 3e–i) and TEM images (Fig. 2b and e) of intermediates, it is apparent that "Path a" is a better mechanism to describe the growth of ZnO micronuts.

The influence of synthesis temperature on the appearance of ZnO crystallites is depicted in Fig. 5. The FE-SEM images of the final products collected after 24 h of synthesis at (a) 180 °C, (b) 190 °C and (c) 200 °C ($Zn(NO_3)_2{\cdot}6H_2O$ molarity = 0.1 M) reveal that with the rise of temperature, there is improvement in crystallinity and surface smoothness. It is envisaged that the growth process is controlled by structural as well as energetic factors. It is apparent that in the shape of a nut, the energy of the system remains at its lowest level during the growth process. In the final stage, the open gap on the nut surface fuses up to reach minimal surface energy.

The effect of $Zn(NO_3)_2{\cdot}6H_2O$ molarity on the morphology of final product (synthesized at 150 °C for 24 h) is shown in Fig. 6. At 0.01 M, ZnO microcrystals with nanorods growing on the base of the half nuts are detected as majority; there is occasional sighting of long micronuts with sharp ends and smooth surfaces (Fig. 6a). It seems that Path b of Fig. 4 is more suitable to describe the growth of this kind of micronuts. At 0.03 M (Fig. 6b), spherical microcrystals are formed (as majority) and entities that detected in Fig. 6a can also be seen. The formation of spherical microcrystals is likely to be a result of isotropic growth around nuclei as suggested by Jung et al. [19]. At 0.05 M (Fig. 6c), there is the detection of brushlike assemblies and hexagonal rods together with those entities sighted in Fig. 6a. The formation of brushlike entities was reported before by Li et al. [20]. The hierarchical structure is a result of preferential growth of ZnO along the $\langle 0\,0\,0\,1\rangle$ direction, with the surface of the resulted nanorod serving as seed layer [18] for the growth of nanowires.

At 0.08 M, there is sighting of popcornlike entities (Fig. 6d). As the molarity of $Zn(NO_3)_2{\cdot}6H_2O$ is getting close to 0.1 M, it is apparent that the "Path a" mechanism depicted in Fig. 4 is favored. The popcornlike entities are generated as a result of two ZnO half nuts growing together at the sharp ends. At 0.5 M (Fig. 6e), we detected twin hexagonal microprisms that are joint together. The surface of this kind of ZnO microcrystal is smooth and its length is up to 20 μm. Twin hexagonal microlayers of shorter length can be seen (indicated by arrows in Fig. 6e). It is possible that further growth of twin hexagonal microlayers would result in the formation of twin hexagonal microprisms. The twin hexagonal microprisms evolving from hexagonal bilayer disks were reported before by Zhang et al. [14]. At 1 M (Fig. 6f), we detect irregular porous ZnO microcrystals. Based on the discussion of Fig. 6, the samples obtained at $Zn(NO_3)_2{\cdot}6H_2O$ molarity of 0.08, 0.1 and 0.5 M gave uniform morphologies. In summary, by means of adopting $Zn(NO_3)_2{\cdot}6H_2O$ of specific molarity, one can fabricate ZnO microcrystals of various shapes through the solvothermal approach.

The room-temperature optical properties of the as-synthesized ZnO microcrystals were studied. Fig. 7I depicts the UV–vis absorption spectra of ZnO microcrystals synthesized at 150 °C for 24 h at different $Zn(NO_3)_2{\cdot}6H_2O$ molarities. The difference in extent of UV absorption is due to variation in sample mass. It is clear that all the materials exhibit excitonic absorption edges around 376 nm. Compared to that of bulk ZnO (370 nm) [21], there is a modest red shift of around 6 nm attributable to size effect and/or the special morphologies of the microcrystals [22]. Shown in Fig. 7II are the room-temperature PL spectra of ZnO microcrystals synthesized at $Zn(NO_3)_2{\cdot}6H_2O$ molarity of (a) 0.1 and (b) 0.01 M; the FE-SEM images of the corresponding products are shown in Figs. 3i and 6a. At 0.1 M, ZnO microcrystals in the shape of acorn are formed, whereas at 0.01 M, half nuts with nanorods growing on the bases are detected. In both cases, bands are detected at around 390, 580 and 630 nm (Fig. 7II). The near-band-edge UV signal (390 nm) is due to free exciton emission [23]. It is known that during the growth of crystals in self-aggregation processes at low temperatures or during the conversion of zinc oxyhydroxide species to ZnO arrays (likely to be nonstoichiometric), there is the formation of structural defects such as stacking faults and dislocations [24,25]. The green emission at 580 nm is commonly related to these kinds of defects and attributed to the recombination of electrons in oxygen vacancies. The 630 nm band can be related to the combination of photogenerated holes and singly ionized electrons located at oxygen vacancies [26]. Since the positions of the PL bands in these two cases are similar, one can deduce that a change of $Zn(NO_3)_2{\cdot}6H_2O$

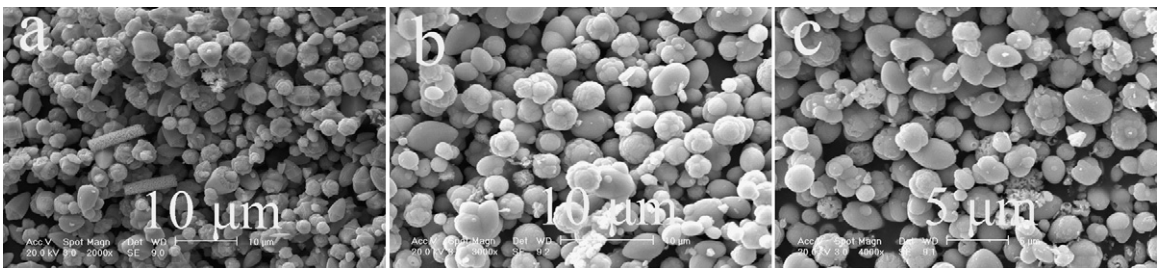

Fig. 5. Morphology of ZnO micronuts synthesized at different temperatures: (a) 180 °C, (b) 190 °C and (c) 200 °C ($Zn(NO_3)_2{\cdot}6H_2O$ molarity = 0.1 M and time = 24 h).

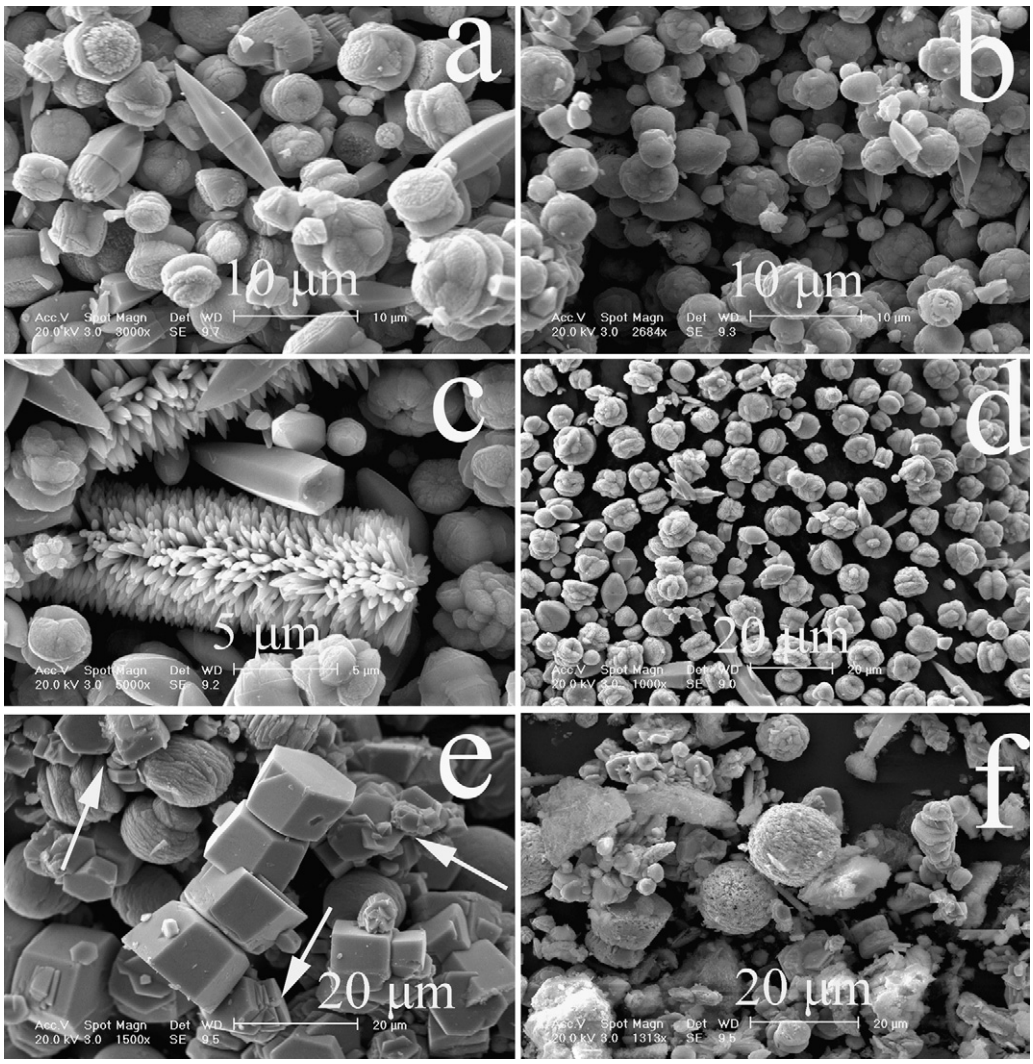

Fig. 6. SEM images of ZnO microcrystals synthesized at 150 °C for 24 h at different $Zn(NO_3)_2{\cdot}6H_2O$ molarities: (a) 0.01 M, (b) 0.03 M, (c) 0.0 5 M, (d) 0.08 M, (e) 0.5 M and (f) 1 M. (Indicated arrows are the ZnO twin hexagonal microlayers.)

concentration from 0.01 to 0.1 M has little effect on the crystallinity and defect nature of the fabricated ZnO microcrystals.

It is worth emphasizing that the solvothermal method described in this paper is better than the conventional oil–water surfactant one. The former is simple, efficient and $Zn(NO_3)_2{\cdot}6H_2O$ is non-toxic and relatively cheap. Furthermore, the alcohol system is biosafe and environment-benign. The work will open up new dimensions for the development of environment-benign methods for the preparation and assembly of novel single-crystalline nanostructures in a rational manner. It is envisaged that the approach can be used to synthesize nanostructures of other oxides such as FeO and MgO.

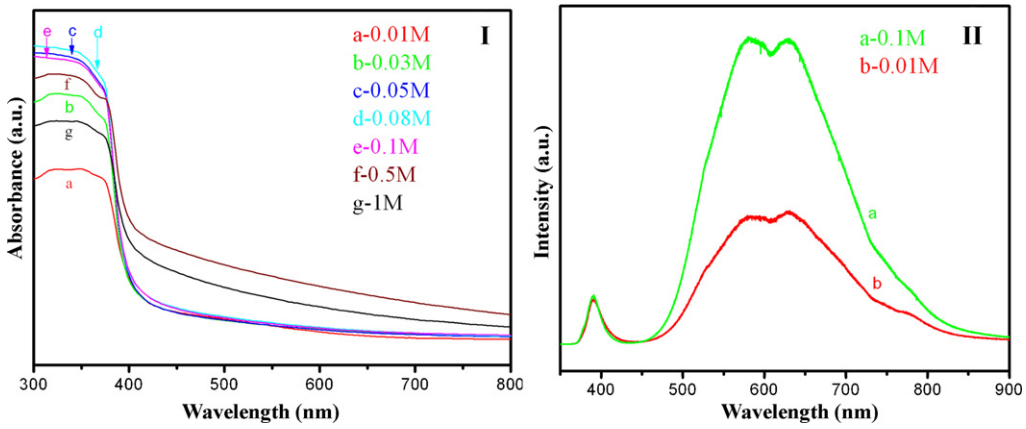

Fig. 7. (I) UV–vis absorption and (II) PL spectra of ZnO microcrystals synthesized at 150 °C for 24 h at different molarities of $Zn(NO_3)_2{\cdot}6H_2O$.

4. Conclusion

By means of the described solvothermal approach that is environment-friendly, facile and low-cost, ZnO microcrystals can be synthesized from $Zn(NO_3)_2{\cdot}6H_2O$. By adjusting parameters such as reaction time, temperature and reactant concentration, ZnO microcrystals that are different in shape can be fabricated in high selectivity. They can be spherical or in the form of flowers, nuts, hexagon-pillars, popcorns and brushes. The FE-SEM results show that the nutlike ZnO microcrystals are composed of self-assembled nanorods that grow on layers of transient ($Zn_5(OH)_8(NO_3)_2(H_2O)_2$) or $Zn(OH)_2$. We find that all the ZnO microcrystals are similar in excitonic absorption edge and PL properties. We envisage that the method is also suitable for the synthesis of nanostrucures of other oxides (such as MgO, FeO).

Acknowledgments

We would like to thank the Foundation of National Laboratory of Solid State Microstructures, Nanjing University (grant no. 2010ZZ18), and the National Key Project for Basic Research (grant nos. 2011CB922102 and 2010CB923402), People's Republic of China, for financial support.

References

[1] J.H. Kim, D. Andeen, F.F. Lange, Adv. Mater. 18 (2006) 2453.
[2] Z.X. Yang, W. Zhong, Y.X. Yin, X. Du, Y. Deng, C.T. Au, Y.W. Du, Nanoscale Res. Lett. 5 (2010) 961.
[3] N. Saito, H. Haneda, T. Sekiguchi, N. Ohashi, I. Sakaguchi, K. Koumoto, Adv. Mater. 14 (2002) 418.
[4] A.R. Hutson, Physica Rev. Lett. 4 (1960) 505.
[5] T. Sivakumar, K. Shanthi, T. Newton Samuel, Bioprocess Eng. 23 (2000) 579.
[6] D. Wang, X.F. Chu, M.L. Gong, Nanotechnology 18 (2007) 185601.
[7] (a) HuangF M.H., Y.Y. Wu, H. Feick, N. Tran, E. Weber, P.D. Yang, Adv. Mater. 13 (2001) 113;
(b) Z.W. Pan, Z.R. Dai, Z.L. Wang, Science 291 (2001) 1947;
(c) Z. Gui, J. Liu, Z.Z. Wang, L. Song, Y. Hu, W.C. Fan, D.Y. Chen, J. Phys. Chem. B 109 (2005) 1113;
(d) M. Salavati-Niasari, N. Mir, F. Davar, J. Alloys Compd. 476 (2009) 908;
(e) X.Y. Kong, Y. Ding, R. Yang, Z.L. Wang, Science 303 (2004) 1348;
(f) W.L. Hughes, Z.L. Wang, J. Am. Chem. Soc. 126 (2004) 6703;
(g) J.H. Yang, J.H. Zheng, H.J. Zhai, L.L. Yang, Y.J. Zhang, J.H. Lang, M. Gao, J. Alloys Compd. 475 (2009) 741;
(h) Hao Jiang, J.Q. Hu, F. Gu, C.Z. Li, J. Alloys Compd. 478 (2009) 550.
[8] P.X. Gao, Y. Ding, W.J. Mai, W.L. Hughes, C.S. Lao, Z.L. Wang, Science 309 (2005) 1700.
[9] M.H. Huang, S. Mao, H. Feick, H.Q. Yan, Y.Y. Wu, H. Kind, E. Weber, R. Russo, P.D. Yang, Science 292 (2001) 1897.
[10] J.L. Yang, S.J. An, W.I. Park, G.C. Yi, W. Choi, Adv. Mater. 16 (2004) 1661.
[11] Y. Sun, G.M. Fuge, M.N.R. Ashfold, Chem. Phys. Lett. 396 (2004) 21.
[12] C. Liu, J.A. Zapien, Y. Yao, X. Meng, C.S. Lee, S. Fan, Y. Lifshitz, S.T. Lee, Adv. Mater. 15 (2003) 838.
[13] Y. Zeng, T. Zhang, W.Y. Fu, Q.J. Yu, G.R. Wang, Y.Y. Zhang, Y.M. Sui, L.J. Wang, C.L. Shao, Y.C. Liu, H.B. Yang, G.T. Zou, J. Phys. Chem. C 113 (2009) 8016.
[14] X.L. Zhang, R. Qiao, R. Qiu, J.C. Kim, Y.S. Kang, Crystal Growth Des. 9 (2009) 2907.
[15] Z.X. Yang, W. Zhong, C.T. Au, X. Du, H.A. Song, X.S. Qi, X.J. Ye, M.H. Xu, Y.W. Du, J. Phys. Chem. C 113 (2009) 21269.
[16] U.K. Gautam, L.S. Panchakarla, B. Dierre, X.S. Fang, Y. Bando, T. Sekiguchi, A. Govindaraj, D. Golberg, C.N.R. Rao, Adv. Funct. Mater. 19 (2009) 131.
[17] K. Govender, D.S. Boyle, P.B. Kenway, P.J. O'Brien, J. Mater. Chem. 14 (2004) 2575.
[18] E. Greene, M. Law, D.H. Tan, M. Montano, J. Goldberger, G. Somorjai, P.D. Yang, Nano Lett. 5 (2005) 1231.
[19] S.H. Jung, E. Oh, K.H. Lee, Y. Yang, C.G. Park, W. Park, S.H. Jeong, Crystal Growth Des. 8 (2008) 265.
[20] X.Y. Li, F.H. Zhao, J.X. Fu, X.F. Yang, J. Wang, C.L. Liang, M.M. Wu, Crystal Growth Des. 9 (2009) 409.
[21] Y.X. Liu, Y.C. Liu, C.L. Shao, R. Mu, J. Phys. D: Appl. Phys. 37 (2004) 3025.
[22] P.K. Samanta, S.K. Patra, P. Roy Chaudhuri, Phys. E 41 (2009) 664.
[23] Y.C. Kong, D.P. Yu, B. Zhang, W. Fang, S.Q. Feng, Appl. Phys. Lett. 78 (2001) 407.
[24] S. Sepulveda-Guzman, B. Reeja-Jayanc, E. de la Rosad, A. Torres-Castro, V. Gonzalez-Gonzalez, M. Jose-Yacamane, Mater. Chem. Phys. 115 (2009) 172.
[25] A.D. Dijken, E.A. Meulenkamp, D. Vanmaekelbergh, A. Meijerink, J. Phys. Chem. B 104 (2000) 1715.
[26] J.Q. Hu, Y. Bando, J.H. Zhan, Y.B. Li, T. Sekiguchi, Appl. Phys. Lett. 83 (2003) 21.